Science of the Total Environment 806 (2022) 150502

Contents lists available at ScienceDirect

Science of the Total Environment

journal homepage: www.elsevier.com/locate/scitotenv

High atmospheric wet nitrogen deposition and major sources in two cities of Yangtze River Delta: Combustion-related NH_3 and non-fossil fuel NO_x

Zhili Chen [a], Xiaohu Huang [a], Changchun Huang [a,b,c,d], Yanju Yang [e], Hao Yang [a], Jinbo Zhang [a], Tao Huang [a,b,c,d,*]

[a] School of Geography Science, Nanjing Normal University, Nanjing 210023, PR China
[b] Jiangsu Center for Collaborative Innovation in Geographical Information Resource Development and Application, Nanjing Normal University, Nanjing 210023, PR China
[c] Key Laboratory of Virtual Geographic Environment (Nanjing Normal University), Ministry of Education, Nanjing 210023, PR China
[d] State Key Laboratory Cultivation Base of Geographical Environment Evolution (Jiangsu Province), Nanjing 210023, PR China
[e] College of Environmental Science and Engineering, Yangzhou University, Yangzhou 225000, China

HIGHLIGHTS

- Rates and sources of wet N deposition were investigated in the Yangtze River Delta.
- NH_3 from combustion sources was higher than that from volatilization sources.
- NO_x from non-fossil fuel emissions was comparable to fossil-fuel combustion.
- $\delta^{15}N$ values of precipitation NH_4^+ increased with increasing precipitation pH.

GRAPHICAL ABSTRACT

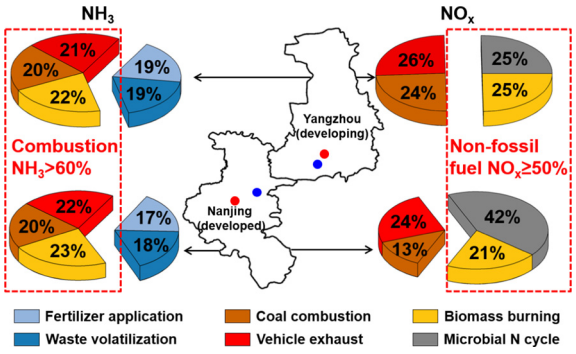

ARTICLE INFO

Article history:
Received 16 July 2021
Received in revised form 12 September 2021
Accepted 17 September 2021
Available online 23 September 2021

Editor: Pingqing Fu

Keywords:
Nitrogen deposition
Stable nitrogen isotopes
Ammonium
Nitrate
Bayesian isotope mixing model

ABSTRACT

High ammonia (NH_3) and nitrogen oxide (NO_x) emissions are related to serious air pollution in urban areas and the negative impacts of excessive reactive nitrogen (N) deposition on many ecosystems. However, whether there is a relationship between N deposition rates and their sources with urbanization or not remains unclear in many areas. Here, we investigated the deposition rates of ammonium (NH_4^+), nitrate (NO_3^-), dissolved organic N, and water-insoluble particular N from July 2017 to June 2018 at two urban and two suburban sites in the Yangtze River Delta (YRD). The $\delta^{15}N$ values of precipitation NH_4^+ and NO_3^- were measured, and major sources were analyzed using a Bayesian isotope mixing model. Wet N deposition rates were higher in Yangzhou (developing city, 20.3–22.7 kg N ha^{-1} yr^{-1}) than those in Nanjing (developed city, 19.4–20.5 kg N ha^{-1} yr^{-1}), and were higher at urban sites (20.4–22.5 kg N ha^{-1} yr^{-1}) than those at suburban sites (18.7–20.3 kg N ha^{-1} yr^{-1}). $\delta^{15}N$ values of precipitation NH_4^+ increased with an increase in precipitation pH because ambient acidity affects the equilibrium isotope fractionation between NH_3 and NH_4^+ and wet scavenging coefficients of NH_3 and particulate NH_4^+. For NH_4^+, combustion-related NH_3 sources (62%–65% with 5.5–6.4 kg N ha^{-1} yr^{-1}, including coal combustion, vehicle exhaust, and biomass burning) contributed more than volatilization NH_3 sources (35%–38% with 2.9–3.9 kg N ha^{-1} yr^{-1}, including fertilizer application and waste volatilization). For NO_3^-, non-fossil fuel NO_x sources (50%–63% with 3.4–4.1 kg N ha^{-1} yr^{-1}, including biomass burning and

Abbreviations: YRD, Yangtze River Delta; BTH, Beijing-Tianjin-Hebei; PRD, Pearl River Delta; SIAR, Stable Isotope Analysis in R; SY, Suiyuan; XL, Xianlin; HHC, Hehuachi; YZJ, Yangzijin; TN, total N; TDN, total dissolved N; DON, dissolved organic N; WIPN, water-insoluble particulate N; VWM, volume-weighted mean; NRS, non-rainy season; RS, rainy season.

* Corresponding author at: School of Geography Science, Nanjing Normal University, Nanjing 210023, PR China.
E-mail address: 09392@njnu.edu.cn (T. Huang).

https://doi.org/10.1016/j.scitotenv.2021.150502
0048-9697/

microbial N cycle) were comparable to fossil fuel NO_x sources (37%–50% with 2.4–3.4 kg N ha^{-1} yr^{-1}, including coal combustion and vehicle exhaust). This study evidenced high N deposition rates and the importance of combustion-related NH_3 emissions and non-fossil fuel NO_x emissions in city areas of the YRD.

1. Introduction

The increase in human activity since the 19th century, including urbanization, industrialization, and high-intensity cultivation, has led to a rapid increase in anthropogenic reactive nitrogen (N) emissions (Galloway et al., 2008; Fowler et al., 2013; Yu et al., 2019). Reactive N undergoes atmospheric reactions and circulation, deteriorates air quality, and eventually returns to the surface ecosystem through dry and wet N deposition (Fowler et al., 2013). Excessive atmospheric N deposition results in aquatic eutrophication, soil acidification, and biodiversity loss (Liu et al., 2013; Gu et al., 2015). China as an N deposition hotspot region (Galloway et al., 2008), has been suffering from serious atmospheric N pollution and a large increase in N deposition rate, average of 0.18–0.41 kg N ha^{-1} yr^{-1} (Liu et al., 2013; Lu and Tian, 2014). Therefore, budgeting N deposition rates and identifying/categorizing N emission sources are crucial for understanding the N cycle and effectively reducing the negative effects of N deposition.

Previous emission inventories indicated that livestock manure and fertilizer application accounted for 48%–55% and 33%–40% of total ammonia (NH_3) emissions in the Yangtze River Delta (YRD; including Nanjing and Yangzhou city) (Huang et al., 2011; Fu et al., 2013), respectively. However, recent studies have indicated that urban areas are the hotspot of NH_3 emissions, and the emission density is an order of magnitude higher than that in rural areas (Meng et al., 2017; Pan et al., 2018a), possibly due to non-agricultural NH_3 sources (Chang, 2014). For example, human excreta (Chang et al., 2015) and vehicle exhaust (Chang et al., 2016a) account for 11.4% and 12.0% of total NH_3 emissions in Shanghai, another megacity of the YRD, respectively. Moreover, the contribution of biomass burning to atmosphere NH_3 or ammonium (NH_4^+) cannot be neglected (Liu et al., 2017; Cui et al., 2018). Regarding nitrogen oxides (NO_x), bottom-up emission inventories indicate that fossil-fuel emissions account for more than 88% of the total NO_x emissions (Ohara et al., 2007; Anenberg et al., 2017). In contrast, recent results indicate that biomass burning and soil emissions account for 20% and 22% of global NO_x emissions, respectively, based on atmospheric chemical transport and terrestrial models (Martin, 2003; Jaeglé et al., 2005; Jain et al., 2006). The integration of bottom-up spatial models and top-down airborne observations indicated that agricultural soil NO_x emissions account for 20%–51% of the total NO_x emissions in California, USA (Almaraz et al., 2018). Furthermore, isotope mass balance suggests that non-fossil fuel emissions account for 55% ± 7% of the total NO_x emissions in East Asia, North America, and Europe (Song et al., 2021).

Because of the presence of numerous NH_3 and NO_x sources, as noted above, the accurate identification of source apportionments is difficult. Stable N isotopes ($\delta^{15}N$) facilitate identification of major emission sources because different sources have different $\delta^{15}N$ values (Table S1); $\delta^{15}N$ quantification through a stable isotopic mixing model has revealed the relative contribution of different sources to atmospheric N (Liu et al., 2017; Pan et al., 2018b; Ti et al., 2018). However, there are two considerable uncertainties that arise when using stable N isotopes: the $\delta^{15}N$ values of emission sources and the N isotope fractionation during the formation of NH_4^+ and nitrate (NO_3^-) (Liu et al., 2017). The $\delta^{15}N$ values of NH_3 and NO_x emissions are still limited and have substantial variabilities (Table S1). The kinetic isotope fractionation during the unidirectional reaction and the equilibrium isotope fractionation during the reversible reaction result in the $\delta^{15}N$ value of particulate N (i.e., NH_4^+ and NO_3^-) being significantly higher than that of gaseous precursors (i.e., NH_3, nitrogen dioxide (NO_2), and nitric acid (HNO_3)) (Heaton et al., 1997; Zheng et al., 2018; Liu et al., 2020). Precipitation can efficiently scavenge gaseous and particulate N species from the atmosphere via rainout and washout processes (Mizak et al., 2005; Seinfeld and Pandis, 2006). However, the different wet scavenging coefficients of gaseous and particulate N species result in the difference between $\delta^{15}N$ values of precipitation and $\delta^{15}N$ values of the initial mixture (NH_3 or NO_x) from different emission sources (Zheng et al., 2018; Liu et al., 2020; Song et al., 2021). Some researchers have reported that isotope fractionation can be neglected (Chang et al., 2016b; Liu et al., 2017; Cui et al., 2018), whereas others have suggested that it should be considered (Wang et al., 2017; Pan et al., 2018b; Ti et al., 2018; Huang et al., 2019) and that the relative contributions of different sources vary with different fractionation scenarios (Huang et al., 2019). Previous studies (Xiao et al., 2012; Xiao et al., 2015; Ti et al., 2018) have reported the factors that affect $\delta^{15}N$ fractionation in rainwater, such as precipitation, rainfall intensity, temperature, and relative humidity; however, the effect of pH on N isotopes has rarely been reported (Moore, 1977; Li et al., 2012a). Detailed investigation is necessary for characterizing isotopic fractionation under various atmospheric neutralization conditions, which would aid the interpretation of isotopic data and elucidate N dynamics in the atmosphere.

Due to high population, cities experience more serious negative effects caused by N pollution and elevated N deposition (Pan et al., 2018a; Decina et al., 2019). The YRD, the Beijing-Tianjin-Hebei region (BTH), and the Pearl River Delta (PRD) are three important urban agglomerations in China, experiencing rapid economic growth and urbanization. In the present study, we observed atmospheric wet N deposition and its stable N isotope on the basis of rain events at urban and suburban sites of developed and developing cities in the YRD. The objectives of this study were: (1) to reflect the effect of urbanization on wet N deposition; (2) to evaluate the influence of precipitation pH on $\delta^{15}N$ values of precipitation NH_4^+; and (3) to attempt to partition NH_3 and NO_x sources by considering N isotopic fractionation.

2. Materials and methods

2.1. Sampling site

This study was conducted in both a developed city (Nanjing) and a developing city (Yangzhou). The proportion of urban population to the total population (88.3%), total gross domestic product (GDP) (1171.5×10^9 RMB), per capita GDP (141,103 RMB), and per capita disposable income (54,538 RMB) of Nanjing are substantially higher than those of Yangzhou (Table S2). Four monitoring sites—Suiyuan (SY), Xianlin (XL), Hehuachi (HHC), and Yangzijin (YZJ)—were selected to represent the urban and suburban areas of Nanjing and Yangzhou (Fig. 1). SY (32°03′ N, 118°47′ E) and HHC (32°24′ N, 119°26′ E) are near the center of Nanjing City and Yangzhou City, respectively, and are close to the main roads and densely populated residential and commercial districts. XL (32°07′ N, 118°55′ E) and YZJ (32°21′ N, 119°24′ E) are located in the university towns of Nanjing and Yangzhou, respectively, mainly in the cultural and educational areas and residential areas. Nanjing and Yangzhou have a typical subtropical monsoon climate, with an annual mean temperature of 15 °C and an annual mean rainfall of 1050 mm. Local meteorological parameters were obtained using a portable weather station (RainWise Inc., USA). There was no significant difference in the monthly precipitation and average temperature of the four sampling sites (Fig. 2 a–d).

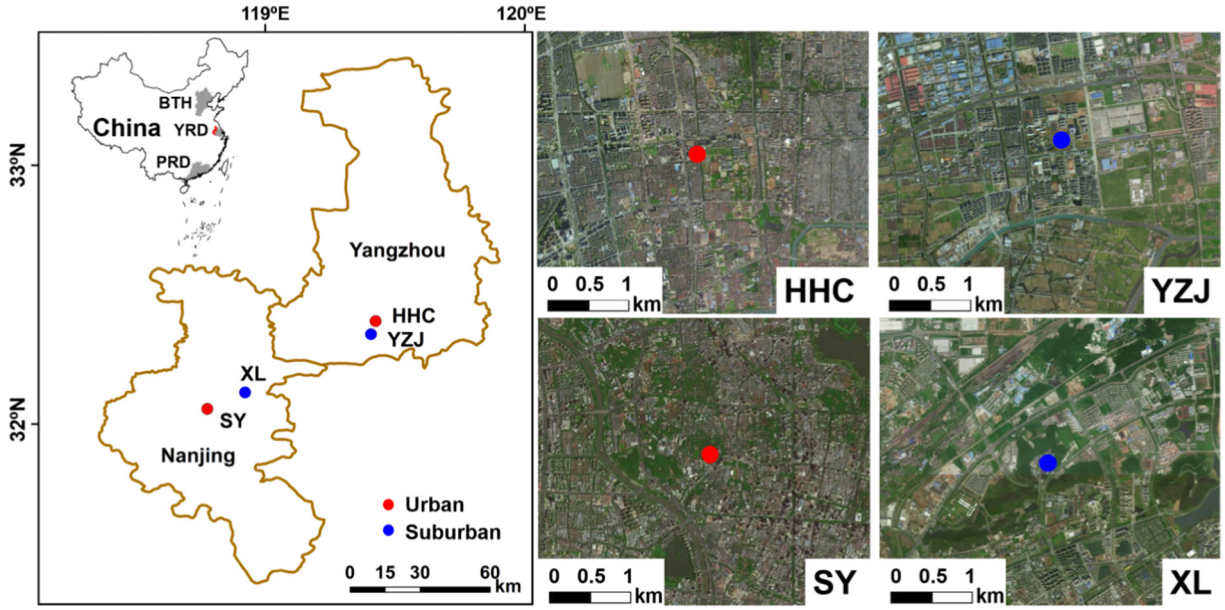

Fig. 1. Location of the study area and sampling sites in Nanjing and Yangzhou. The image of each site is derived from Google Earth. The YRD, the BTH, and the PRD are three important urban agglomerations in East China. YRD: the *Yangtze River Delta*, BTH: *the Beijing-Tianjin-Hebei region*, PRD: *the Pearl River Delta*, SY: *Suiyuan*, XL: *Xianlin*, HHC: *Hehuachi*, YZJ: *Yangzijin*.

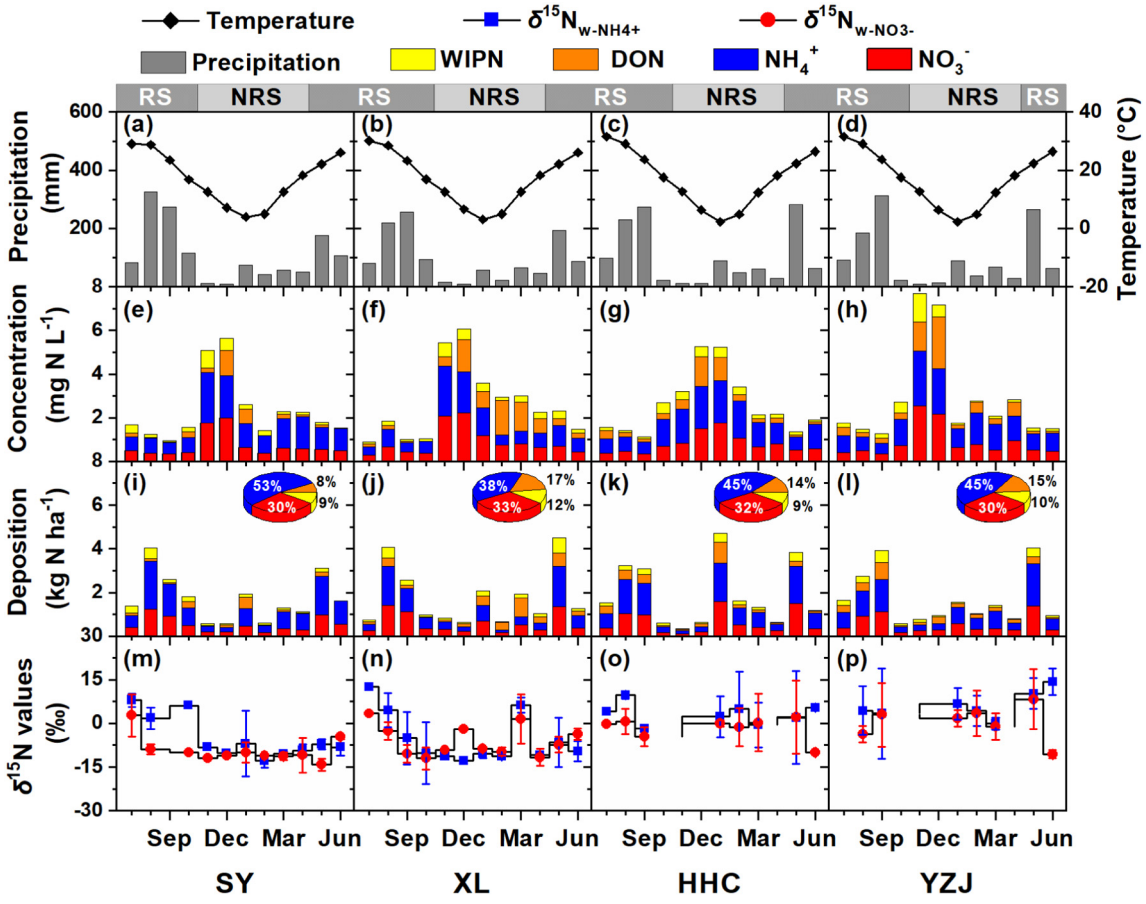

Fig. 2. Monthly precipitation and average temperature (a–d); volume-weighted mean concentration of NH_4^+, NO_3^-, DON, and WIPN (e–h); wet deposition rates and fractional contributions of NH_4^+, NO_3^-, DON, and WIPN (i–l); and mean ± SD values of $\delta^{15}N_{w\text{-}NH4+}$ and $\delta^{15}N_{w\text{-}NO3-}$ (m–p) at SY, XL, HHC, and YZJ in Yangtze River Delta. SY: *Suiyuan*, XL: *Xianlin*, HHC: *Hehuachi*, YZJ: *Yangzijin*, RS: *rainy season*, NRS: *non-rainy season.*

2.2. Sample collection and chemical analyses

Precipitation samples were collected for each rain episode using a wet-only auto-sampler (ZJC-V, Zhejiang Hengda Instrument & Meter Co. Ltd., Hangzhou, China) from July 2017 to June 2018. There were 56, 56, 62, and 63 rainwater samples collected at SY, XL, HHC, and YZJ, respectively. Rainwater samples were collected in 125 mL polytetrafluoroethylene (PTFE) plastic bottles and immediately stored at 4 °C until chemical analyses were conducted.

All rainwater samples were analyzed for total N (TN), total dissolved N (TDN), NH_4^+, and NO_3^- using UV-3600 spectrophotometer (Shimadzu UV-VIS-NIR spectrophotometer, Shimadzu Co., Kyoto, Japan). Dissolved organic N (DON) and water-insoluble particulate N (WIPN) were estimated from the concentration difference between TDN and inorganic N (IN, the sum of NH_4^+ and NO_3^-) and that between TN and TDN, respectively. Each rainwater sample has analyzed the concentration of N species to calculate the monthly volume-weighted mean (VWM) concentration and wet N deposition rate (Fig. 2). A detailed description of the methods for measuring N species concentration and the calculated wet N deposition rate has been provided in previous studies (Chen et al., 2019). The pH of all samples was immediately measured after collection using a pH meter (S400—K, Mettler Toledo, Switzerland). The concentrations of ions were determined using an ion chromatography system [ICS-2000 for cations (F^-, Cl^-, NO_3^-, and SO_4^{2-}) and ICS-3000 system for anions (Na^+, NH_4^+, K^+, Mg^{2+}, and Ca^{2+}) (Dionex Co., Sunnyvale, CA, USA)]. The concentrations of ions were used to analyze the ion correlation at Nanjing and Yangzhou (Table S3).

The $\delta^{15}N$ values of precipitation NH_4^+ and NO_3^- ($\delta^{15}N_{w\text{-}NH4+}$ and $\delta^{15}N_{w\text{-}NO3-}$, respectively) were measured using the diffusion method as described in previous studies (Sigman et al., 1997; Zhang et al., 2017; Cao et al., 2018). To ensure that the amounts of NH_4^+ and NO_3^- in the sample were both greater than 100 μg N, an additional 500 mL event-based rainwater sample was concentrated to 20 mL at −50 °C (Scientz-N, Ningbo Xinzhi Biotechnology Co., Ltd.). There is enough volume of rainwater for N isotope analysis when the rainfall is more than 6 mm. There are 10 out of 26 samples, 11 out of 27 samples, 12 out of 24 samples, 11 out of 24 samples for N isotope analysis during non-rainy season at SY, XL, HHC, and YZJ, respectively. A total of 20 mL of concentrated rainwater sample was taken in a 250 mL airtight glass bottle, and magnesium oxide was added to convert NH_4^+ to NH_3, which was adsorbed by an oxalic acid-spiked filter paper. The recovery rate of NH_4^+ was greater than 95% after incubation of the sample for 24 h at 25 °C on a rotator running at 140 r min^{-1}. The remaining NH_4^+ was removed by a fresh acid-spiked filter paper for incubation for 48 h under the same conditions before determining the $\delta^{15}N$ values of NO_3^-. The used filter paper was replaced with two new acid-spiked ones, and 0.3 g Devarda's alloy was added to reduce NO_3^- to NH_4^+. The sample was incubated for 24 h to complete the processes of diffusion and recovery of NO_3^-. The adsorbent filter paper was dried in a desiccator for 48 h, and $\delta^{15}N_{w\text{-}NH4+}$ and $\delta^{15}N_{w\text{-}NO3-}$ values$^-$ were measured using an isotope ratio mass spectrometer (Thermo Fisher Scientific Delta V Plus). Three international standards, namely USGS25 ($\delta^{15}N = -30.4‰$), IAEA-N-1 ($\delta^{15}N = +0.4‰$), and IAEA-N-2 ($\delta^{15}N = +20.3‰$), were used to calculate $\delta^{15}N_{w\text{-}NH4+}$. Three international standards, namely USGS32 ($\delta^{15}N = +180.0‰$), USGS34 ($\delta^{15}N = -1.8‰$), and USGS35 ($\delta^{15}N = +2.7‰$), were used to calculate $\delta^{15}N_{w\text{-}NO3-}$. The standard deviations (SD) of the replicate analyses of an individual sample were ± 0.2‰ and ± 0.3‰ for $\delta^{15}N_{w\text{-}NH4+}$ and $\delta^{15}N_{w\text{-}NO3-}$, respectively.

2.3. Source identification and statistical analysis

As noted in the second paragraph of the introduction, we selected five major NH_3 sources, namely, fertilizer application, waste volatilization, vehicular exhaust, coal combustion, and biomass burning. We also selected four major NO_x sources: coal combustion, vehicle exhaust, biomass burning, and microbial N cycle. The $\delta^{15}N$ values of these sources are listed in Table S1. It should be noted that NO_x from the microbial N cycle includes the sum of NO_x from natural and fertilized soils, aquatic ecosystems, urban sewage, and animal wastes in both urban and rural areas. It is noteworthy that $\delta^{15}N$ values of NH_3 from livestock manure, human and pet exhaust, and disposed waste are close and overlap (Chang et al., 2016b; Elliott et al., 2019); thus, these products are universally considered as waste volatilization. The $\delta^{15}N$ values of NH_3 sources based on the passive samplers were calibrated by adding 15‰ to compensate for the systematic low bias of passive samplers in characterizing the $\delta^{15}N$ values of NH_3 (Pan et al., 2020; Walters et al., 2020).

The relative contribution of each source to precipitation NH_4^+ or NO_3^- was calculated using stable isotope analysis in R (SIAR model: http://cran-project.org/web/packages/siar/index.html). This model uses a Bayesian framework to establish a logical prior distribution based on Dirichlet distribution (Evans et al., 2000) and then determines the probability distribution for the source proportions of the mixture (Parnell and Jackson, 2008). It can substantially incorporate the uncertainties associated with multiple sources, fractionations, and measured isotope signatures (Moore and Semmens, 2008; Davis et al., 2015). In this study, uncertainties were considered by input mean ± SD $\delta^{15}N$ values of sources (Table S1) and isotope effects and all replicate values of $\delta^{15}N_{w\text{-}NH4+}$ and $\delta^{15}N_{w\text{-}NO3-}$ into the model, which were expressed as the percentage values of relative contribution (f).

The currently reported isotope effects values for precipitation NH_4^+ and NO_3^- are sparse and vary widely. The isotope effects for precipitation NH_4^+ ranged from 3.4‰ to 20.3‰ with an average of 10.4 ± 4.3‰ based on the Rayleigh model (Xiao et al., 2015). The isotope effects for precipitation NO_3^- averaged 3.9 ± 1.8‰ based on the isotope mass-balance equation (Song et al., 2021). We calculated the relative contributions of major NH_3 and NO_x in the two scenarios (Fig. S1). In scenario 1, there was no isotopic fractionation for precipitation NH_4^+ and NO_3^-. In scenario 2, isotopic fractionation values were 10.4 ± 4.3‰ for NH_4^+ and 3.9 ± 1.8‰ for NO_3^-. Based on the corresponding relative contribution of major sources (f_i, i is the count of major sources) and wet NH_4^+ or NO_3^- deposition rate (D_{NH4+} or D_{NO3-}), the real contribution of major sources (F_i) to the wet NH_4^+ or NO_3^- deposition rate was calculated at each site by $F_i = D_{NH4+} \times f_i$ or $F_i = D_{NO3-} \times f_i$ (Fig. S2).

Statistical analysis was conducted using SPSS version 18.0 (SPSS Inc., Chicago, IL). The Tukey honest significant difference (Tukey HSD) and the least significant difference (LSD) tests of the one-way analysis of variance (ANOVA) were used to identify significant differences in deposition rate between rainy season and non-rainy season, among urban, suburban, and rural, and among YRD, BTH, and PRD (Fig. 3), in $\delta^{15}N$ values of NH_3 or NO_x among major sources (Table S1). Linear regressions were used to examine correlations between precipitation pH and $\delta^{15}N_{w\text{-}NH4+}$ values (Fig. 4). Statistically significant differences were set at $p < 0.05$ or as otherwise stated.

3. Results

3.1. N concentrations in precipitation

The monthly VWM concentrations of NH_4^+, NO_3^-, DON, and WIPN in precipitation showed a similar temporal pattern at the four sites, with higher concentrations in the non-rainy season (NRS; from June to October) and lower concentrations in the rainy season (RS; from November to April) (Fig. 2e–h). The highest concentrations of NH_4^+, NO_3^-, DON, and WIPN were obtained in November or December at the four sites when precipitation was the lowest, while the lowest concentrations were achieved in September (except for July at XL) with high precipitation. The annual VWM concentrations of NH_4^+, NO_3^-, DON, WIPN, and TN (the sum of NH_4^+, NO_3^-, DON, and WIPN) were summarized as 0.61–0.84, 0.49–0.60, 0.12–0.26, 0.16–0.22, and 1.47–1.85 mg N L^{-1}, respectively, showing a small variation across the four sites.

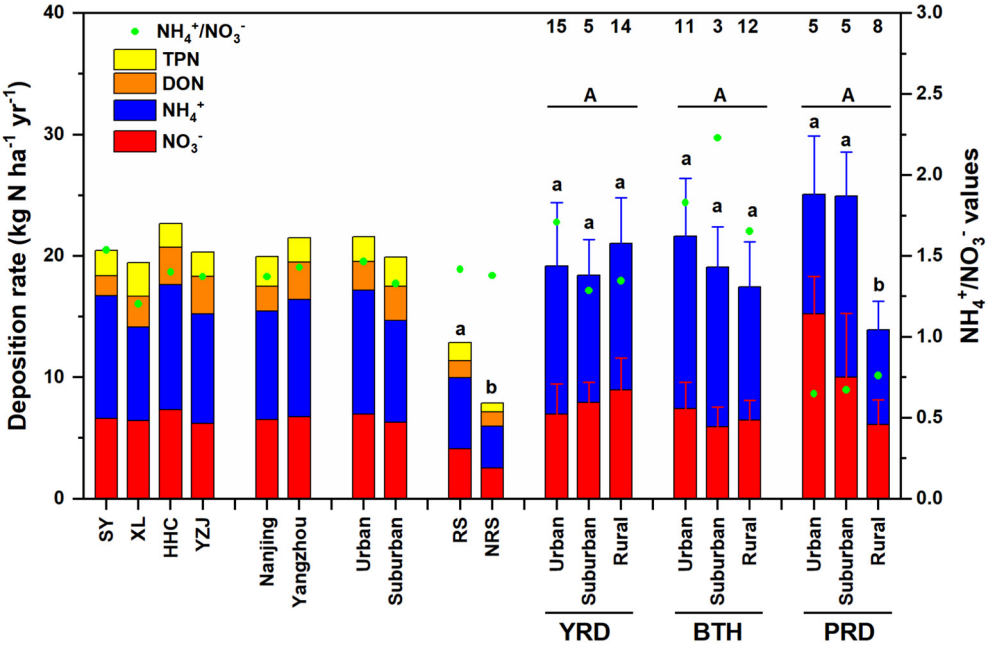

Fig. 3. Wet-only N deposition rate and the NH_4^+/NO_3^- ratio. Nanjing is the mean of SY and XL, Yangzhou is the mean of HHC and YZJ, Urban is the mean of SY and HHC, Suburban is the mean of XL and YZJ, and RS (rainy season, from Jun to Oct) and NRS (non-rainy season, from Nov to Apr) are the mean at the four sites of the corresponding season. Different small letters above the bar stand for a significant difference at the 5% level between RS and NRS and among urban, suburban, and rural. Different capital letters above the bar stand for a significant difference at the 5% level among the Yangtze River Delta (YRD), the Beijing-Tianjin-Hebei region (BTH), and the Pearl River Delta (PRD). The bulk deposition is corrected to wet-only deposition by multiplying by a coefficient of 0.73 (Zhang et al., 2006). Numbers above the bars are those of observation sites (detailed in Table S4).

3.2. Wet N deposition rates

There was no significant ($p > 0.05$) spatial variation in the estimated N deposition rates between cities and locations, which was in the orders of Yangzhou (21.4 kg N ha^{-1} yr^{-1}) > Nanjing (19.5 kg N ha^{-1} yr^{-1}) and urban (21.6 kg N ha^{-1} yr^{-1}) > suburban (19.9 kg N ha^{-1} yr^{-1}) (Fig. 3). There was significant temporal variation in the estimated N deposition rates: the wet TN deposition rate in the RS was significantly higher than that in the NRS ($p < 0.05$) (Fig. 3). The monthly variations in the N deposition rates were similar between cities and locations (Fig. 2i–l). The monthly variation pattern of wet N deposition was consistent with that of precipitation (Fig. 2a–d).

Wet TN deposition was dominated by NH_4^+ and NO_3^-, especially NH_4^+ at the four sites. The proportions of NH_4^+, NO_3^-, DON, and WIPN accounted for TN were 38%–53%, 30%–33%, 8%–17%, and 9%–12%, respectively (Fig. 2i–l). The ratio of NH_4^+ to NO_3^- (NH_4^+/NO_3^-) ranged from 1.2 to 1.5 at the four sites, with spatial and temporal variations similar to those observed for the wet N deposition rate (Fig. 3).

3.3. $\delta^{15}N_{w\text{-}NH4+}$ and $\delta^{15}N_{w\text{-}NO3-}$ values

During the sampling period, the range of $\delta^{15}N_{w\text{-}NH4+}$ and $\delta^{15}N_{w\text{-}NO3-}$ varied from −20.2‰ to +19.9‰ and from −17.3‰ to +17.8‰, respectively, with no clear seasonal variations for either $\delta^{15}N_{w\text{-}NH4+}$ and $\delta^{15}N_{w\text{-}NO3-}$ (Fig. 2m–p). The annual averages of $\delta^{15}N_{w\text{-}NH4+}$ were −5.6‰, −4.9‰, +3.4‰, and +5.2‰ at SY, XL, HHC, and YZJ, respectively, and those of $\delta^{15}N_{w\text{-}NO3-}$ were −9.0‰, −6.6‰, −1.4‰, and −0.2‰ at SY, XL, HHC, and YZJ, respectively. The annual mean $\delta^{15}N_{w\text{-}NH4+}$ and $\delta^{15}N_{w\text{-}NO3-}$ in Nanjing were significantly lower than those in Yangzhou (Fig. 2m–p). There was a significant positive relationship between event-based $\delta^{15}N_{w\text{-}NH4+}$ values and event-based precipitation pH, and between $\delta^{15}N_{w\text{-}NH4+}$ values and precipitation pH for each site (Fig. 4a & b).

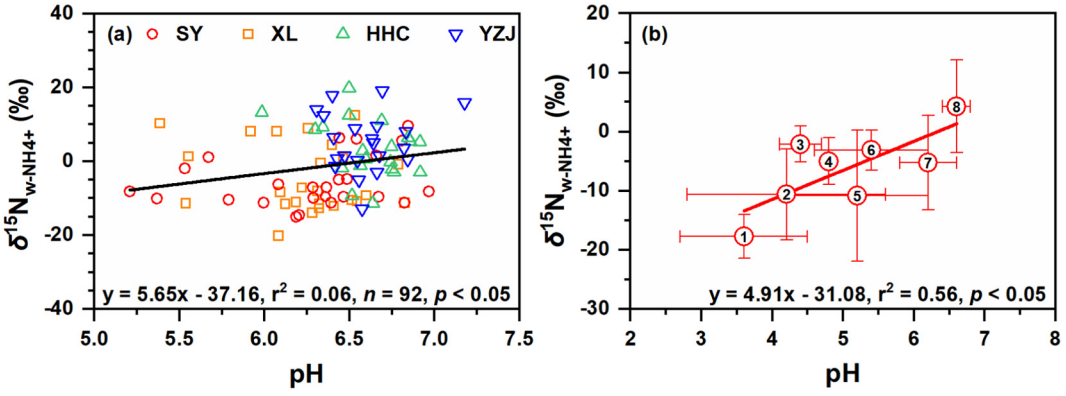

Fig. 4. Relationship between $\delta^{15}N_{w\text{-}NH4+}$ values and precipitation pH at SY, XL, HHC, and YZJ (a) and between site-based mean ± SD $\delta^{15}N_{w\text{-}NH4+}$ values and site-based mean ± SD precipitation pH at urban and suburban sites (b). In panel (b), the numbers in the circles are the data sources. 1: Chengdu, China (Du, 2012); 2: Guiyang, China (Liu et al., 2017; Xiao et al., 2013); 3: Tuckerton, USA (Gao, 2002); 4: Gwangju, Korea (Lee et al., 2012); 5: Beijing, China (Xu and Han, 2009; Liu et al., 2014); 6: Wanzhou, China (Shen et al., 2017; Leng et al., 2018); 7: Nanjing, China (This study); 8: Yangzhou, China (This study).

3.4. Contributions of major sources to precipitation NH_4^+ and NO_3^-

To estimate the major sources contributing to NH_4^+ or NO_3^- in rainwater, $\delta^{15}N_{w\text{-}NH4+}$ or $\delta^{15}N_{w\text{-}NO3-}$ values over the study period were analyzed in the SIAR model and are shown in Fig. 5 & S2. We found that wet NH_4^+ deposition originated more from the combustion-related NH_3 sources (62%–65% with 5.5–6.4 kg N ha^{-1} yr^{-1}) and less from volatilization NH_3 sources (35%–38% with 2.9–3.9 kg N ha^{-1} yr^{-1}). The contributions of coal combustion, vehicle exhaust, biomass burning, fertilizer application, and waste volatilization to NH_4^+ were 19.5%–20.3% (1.5–2.1 kg N ha^{-1} yr^{-1}), 21.6%–22.2% (1.7–2.2 kg N ha^{-1} yr^{-1}), 19.9%–23.6% (1.8–2.3 kg N ha^{-1} yr^{-1}), 16.8%–19.9% (1.3–2.0 kg N ha^{-1} yr^{-1}), and 17.6%–19.9% (1.4–2.0 kg N ha^{-1} yr^{-1}) across the four sites, respectively. Wet NO_3^- deposition originated from non-fossil fuel NO_x sources (50%–63% with 3.4–4.1 kg N ha^{-1} yr^{-1}) were comparable to that from fossil fuel NO_x sources (37%–50% with 2.4–3.4 kg N ha^{-1} yr^{-1}). The contributions of microbial N cycle, biomass burning, coal combustion, and vehicle exhaust to NO_3^- were 24.0%–45.4% (3.4–4.1 kg N ha^{-1} yr^{-1}), 19.7%–25.1% (3.4–4.1 kg N ha^{-1} yr^{-1}), 11.4%–25.0% (3.4–4.1 kg N ha^{-1} yr^{-1}), and 23.5%–25.9% (3.4–4.1 kg N ha^{-1} yr^{-1}) across the four sites, respectively.

4. Discussion

4.1. Wet N deposition rates

The mean wet IN deposition rate of the four sampling sites (15.9 kg N ha^{-1} yr^{-1}) was close to previous results during 2002 and 2017 in the YRD (19.8 kg N ha^{-1} yr^{-1}), and close to that in the developed regions with heavy air pollution in East China: the BTH was 19.4 kg N ha^{-1} yr^{-1} and the PRD was 19.5 kg N ha^{-1} yr^{-1} (Fig. 3). However, it was higher than that of major global N deposition hotspots: USA (3.0–3.5 kg N ha^{-1} yr^{-1}) (Holland et al., 2005; Du et al., 2014; Li et al., 2016), Europe (6.8 kg N ha^{-1} yr^{-1}) (Holland et al., 2005), and higher than that of the background sites in China (2.1–2.7 kg N ha^{-1} yr^{-1}) (Shao et al., 2009; Qiao et al., 2015). The DON deposition rates ranged from 1.6 kg N ha^{-1} yr^{-1} to 3.6 kg N ha^{-1} yr^{-1} and accounted for 8%–17% of TN at the four sites, which was close to previous proportions reported at other urban/suburban sites of China (12%–36% of TDN) (Li et al., 2012b). DON and WIPN deposition contributed 17%–29% of the wet TN deposition at the four sites. Previous studies have underestimated wet N deposition rates by ignoring DON and WIPN. The wet N deposition rate (especially those of NH_4^+ and DON) in Yangzhou was higher than that in Nanjing (Fig. 3) due to differences in the economic structure. The livestock and poultry industrialization, grain production, and fertilizer consumption in Yangzhou were much higher than those in Nanjing (Table S2). Previous studies have indicated that livestock farming and agricultural fertilization are important N sources, accounting for 50% and 35% of the total NH_3 emissions in the YRD, respectively (Huang et al., 2011; Fu et al., 2013).

The wet IN deposition rates in urban areas were higher than those in suburban areas; the same pattern was also found in the YRD, the PRD, and the BTH (Fig. 3). Moreover, IN deposition rates in urban and suburban areas is comparable with that in rural areas of the YRD and the BTH, even significantly higher than that in rural areas of the PRD (Fig. 3). This is consistent with the global spatial variation that cities are subject to higher N deposition than nearby rural areas (Decina et al., 2019), thereby indicating that cities, especially urban areas, are hotspots of N deposition. Urbanization increases the N deposition rate, and more concerted efforts are required to understand the urban N cycle in terms of both sources and effects of urban N deposition. The NH_4^+/NO_3^- values were higher in the studied urban areas than in the suburban areas, which is consistent with previous results in the YRD, indicating that NH_4^+ dominated wet N deposition in the urban areas of the YRD (Fig. 3). The high N deposition rate in the urban areas may be due to non-agricultural NH_3 emissions, such as vehicle emissions, coal combustion products, and exhaust from humans and pets (Chang, 2014; Chang et al., 2015; Chang et al., 2016a; Meng et al., 2017).

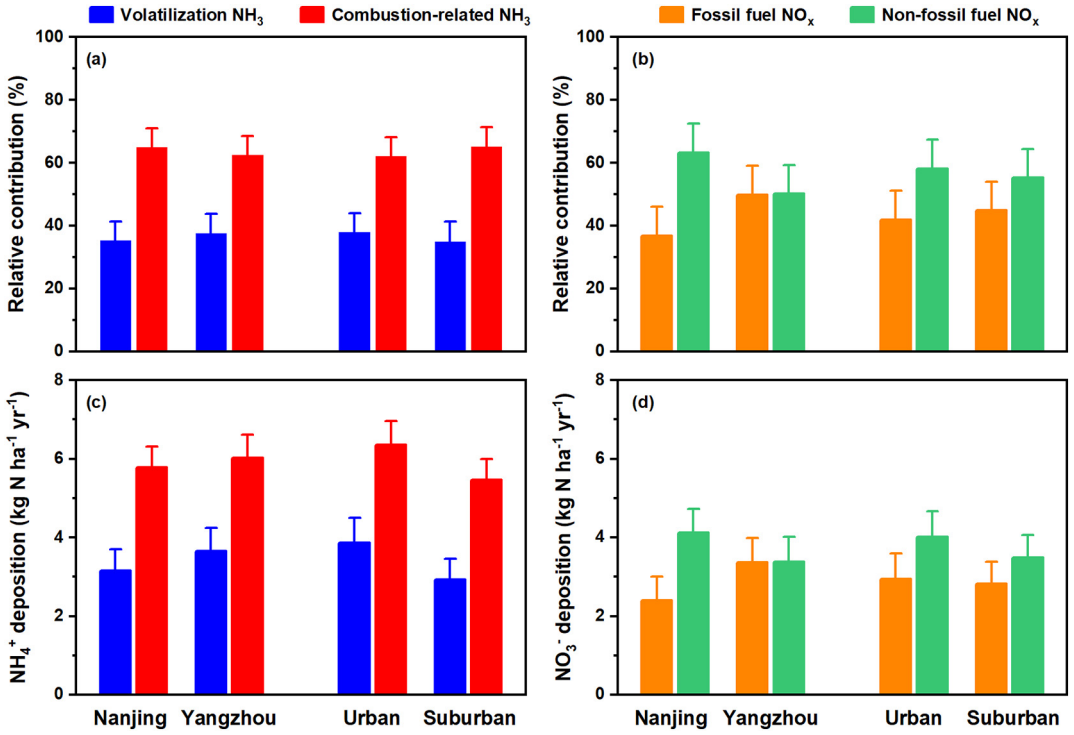

Fig. 5. Relative contribution (a and b) and real contribution (c and d) of volatilization NH_3, combustion-related NH_3, fossil fuel NO_x, and non-fossil fuel NO_x sources to wet NH_4^+ and NO_3^- deposition, respectively. Nanjing is the mean of SY and XL, Yangzhou is the mean of HHC and YZJ, Urban is the mean of SY and HHC, Suburban is the mean of XL and YZJ based on Fig. S2.

4.2. Effect of ambient acidity on NH_4^+ isotope fractionation

The significant positive relationship between precipitation pH and observed $\delta^{15}N_{w\text{-}NH4+}$ values (Fig. 4a & b) may suggest the effect of pH on isotope fractionation. Gaseous NH_3 and particulate NH_4^+ are both captured in raindrops by washout and rainout processes (Mizak et al., 2005; Seinfeld and Pandis, 2006). The acidity may affect the equilibrium isotope fractionation between NH_3 and NH_4^+ and the wet scavenging coefficients of NH_3 and particulate NH_4^+ (Fig. 6).

First, atmospherically reduced N (NH_x) exists as gaseous NH_3 or particulate NH_4^+ depending on the ambient acidity. In an acidic environment, NH_3, as the most important alkaline gas, reacts with H_2SO_4 to form stable ammonium salts ($(NH_4)_2SO_4$ and NH_4HSO_4). In an alkaline environment, excess NH_3 could not be neutralized by acidic precursors or existed as reversible ammonium salts (NH_4NO_3 and NH_4Cl). The diffusion of NH_3 back to the atmosphere during the reversible reaction and strong equilibrium isotope effect between NH_3 and NH_4^+ results in ^{15}N enrichment in particulate NH_4^+ (Zheng et al., 2018; Kawashima, 2019; Walters et al., 2019). The equilibrium isotope fractionation values were 31.0 ± 4.0‰ at 20 °C (Walters et al., 2019) and 35.0‰ at 25 °C (Urey, 1947) based on theoretical calculations. Controlled experiments also indicated equilibrium isotope fractionation values were 33.0 ± 0.2‰ in a closed chamber (Heaton et al., 1997), and 31.6 ± 2.0‰ and 24.0 ± 3.0‰ in a dynamic chamber with a turnover rate of 0.9 and 6.8 times per day, respectively (Kawashima and Ono, 2019). The fractionation values in an acidic environment (i.e., the low molar ratio of NH_3 to NH_4^+; Moore, 1977) were lower than those in an alkaline environment (i.e., the high molar ratio of NH_3 to NH_4^+; Hayasaka et al., 2004; Kawashima, 2019). There was a significantly positive relationship between the $\delta^{15}N$ values of particulate NH_4^+ and the molecular ratio of NH_4^+ to $(NO_3^- + 2 \times SO_4^{2-})$ in Wang et al. (2017). The higher ratio of NH_4^+ to $(NO_3^- + 2 \times SO_4^{2-})$ indicated the incomplete neutralization of ambient NH_3 or the presence of a relatively alkaline environment. If we assume that the relative contribution of NH_3 and particulate NH_4^+ to precipitation NH_4^+ is constant, the lower $\delta^{15}N$ values of particulate NH_4^+ in the acidic environment resulted in lower $\delta^{15}N_{w\text{-}NH4+}$ values. For example, the higher $\delta^{15}N_{w\text{-}NH4+}$ values in summer with equivalent ratios of NH_4^+ to $(NO_3^- + 2 \times SO_4^{2-})$ averaged 1.1, and the lower $\delta^{15}N_{w\text{-}NH4+}$ values in winter with equivalent ratios of NH_4^+ to $(NO_3^- + 2 \times SO_4^{2-})$ averaged 0.5 (Huang et al., 2019).

Second, acidity may affect the relative wet scavenging coefficients of NH_3 and particulate NH_4^+. NH_x is scavenged by cloud water and raindrops either through the dissolution of NH_3 or the absorption of NH_4^+, and then delivered to the surface (Mizak et al., 2005; Seinfeld and Pandis, 2006; Shimshock and Pena, 1988). The in-cloud and under-cloud scavenging mechanisms of particulates include the activation of condensed nuclei under superstation conditions and the collection of aerosols by falling hydrometeors, respectively (Aikawa and Hiraki, 2009). We assume that the interception and absorption of particulate NH_4^+ are not affected by precipitation pH (Liu et al., 2017). However, the dissolution of gaseous NH_3 increases with a decrease in precipitation pH (Li et al., 2012a). Thus, lower precipitation pH may result in lower precipitation $\delta^{15}N_{w\text{-}NH4+}$ due to the increasing dissolution of gaseous NH_3, characterized by the depletion of ^{15}N.

Third, acidity may affect isotope fractionation in the processes of wet scavenging of gaseous NH_3. Previous studies have indicated that more than 88% of the precipitation NH_4^+ in NH_3 pollution areas comes from gaseous NH_3 through below-cloud scavenging (Oberholzer et al., 1993; Mizak et al., 2005). Gaseous NH_3 was absorbed into raindrops through three processes (Xiao et al., 2015) (Fig. 6). The first process is diffusion, which is affected by kinetic fractionation because lighter isotopes have higher diffusion velocity according to the kinetic energy equation. Generally, the rates of diffusion are much higher than that during raindrop removal; hence, equilibrium must be established and the diffusion process can be neglected. The second process is related to the $NH_{3(gas)} \leftrightarrow NH_{3(aq)}$ and $NH_{3(gas)} \leftrightarrow NH_{4(aq)}^+$ equilibria, which were estimated to have an isotope enrichment factor ranging from +20‰ to +27‰ for the $NH_{3(gas)} \leftrightarrow NH_{4(aq)}^+$ equilibrium system and from +5‰ to +15.7‰ for the $NH_{3(gas)} \leftrightarrow NH_{3(aq)}$ equilibrium system (Urey, 1947; Moore, 1977; Hanschmann, 1981; Högberg, 1997; Li et al., 2012a). The third process involves the ionization equilibrium and the absorption process, which results in low or insignificant fractionation (Delwiche and Steyn, 1970; Högberg, 1997). Therefore, isotope fractionation is mainly controlled by equilibrium fractionation in rainwater. Precipitation pH may affect isotope equilibrium fractionation. Nearly all NH_3 will dissolve into the aqueous phase when the pH is lower than 5 (Seinfeld and Pandis, 2006), thus there is no isotopic fractionation between NH_3 and NH_4^+. However, NH_x partly exists as NH_3 and NH_4^+ when the pH is higher than 6 at 25 °C (Li et al., 2012a), resulting in equilibrium isotope fractionation between NH_3 and NH_4^+.

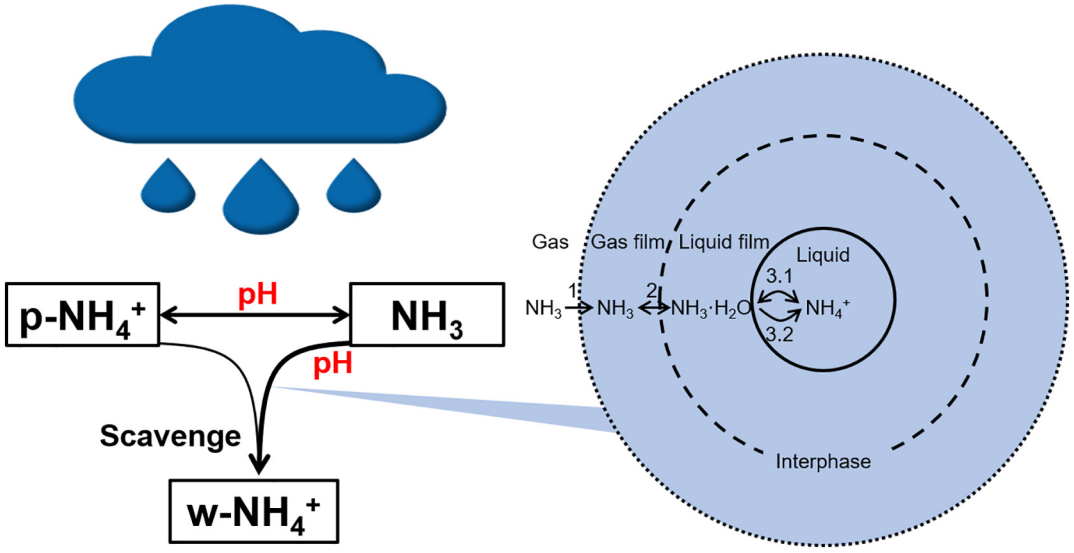

Fig. 6. A schematic of the process of atmospheric NH_x production with zoom-ins for the process of NH_3 transferring from gas to raindrop. The process of NH_3 transferring from gas to raindrop was revised from Xiao et al., 2015. 1. Gaseous diffusion; 2. Gaseous-liquid equilibrium; 3.1. Ionization equilibrium; 3.2 Absorption process. p-NH_4^+: *particulate* NH_4^+; w-NH_4^+: *precipitation* NH_4^+.

4.3. Major sources of NH_4^+ in precipitation

The $\delta^{15}N_{w\text{-}NH4+}$ values in Nanjing ranged from −20.2‰ to +12.5‰ with an average of −5.6 ± 6.9‰ for SY and −4.9 ± 9.1‰ for XL, which fell in the middle range of reported $\delta^{15}N_{w\text{-}NH4+}$ values (Fig. 4b). However, the $\delta^{15}N_{w\text{-}NH4+}$ values ranged from −12.9‰ to +19.9‰ in Yangzhou with an average of +3.4 ± 7.8‰ for HHC and +5.2 ± 8.0‰ for YZJ, which fell in the higher range of reported $\delta^{15}N_{w\text{-}NH4+}$ values and was significantly higher than those in Nanjing (Fig. 4b). The $\delta^{15}N_{w\text{-}NH4+}$ values in Yangzhou exceeded the range of $\delta^{15}N$ for major NH_3 emission sources (−23.3 ~ +12.0‰; Table S1) and could not be explained by the contribution of NH_3 emission sources, suggesting non-negligible isotopic fractionation between initial NH_3 and precipitation NH_4^+.

The pH in Yangzhou averaged 6.6, and 99.2% of samples had pH > 6 (Fig. 4a). The pH values were slightly higher than reported 6.1 during 2002–2003 in the YRD due to the reduction of SO_2 and NO_x emissions in the last decade (Luo et al., 2007). Moreover, there was a significant correlation between Cl^- and NH_4^+ in Yangzhou (Table S3), suggesting that some NH_4^+ existed as reversible ammonium (NH_4Cl). The diffusion of NH_3 back to the atmosphere during the reversible reaction and associated strong equilibrium between NH_3 and NH_4^+ caused significant ^{15}N enrichment in precipitation NH_4^+, thus resulting in considerably higher $\delta^{15}N_{w\text{-}NH4+}$ values in Yangzhou than $\delta^{15}N$ values for potential NH_3 sources and in Nanjing (Table S1). The fractionation factor between gaseous NH_3 and NH_3 or NH_4^+ in precipitation was averaged as 10.4 ± 4.3‰ in Guiyang using the Rayleigh model (Xiao et al., 2015) and was recently applied in the YRD (Ti et al., 2018). If the same fractionation factor was applied in Yangzhou, the expected $\delta^{15}N_{w\text{-}NH4+}$ would range from −23.3‰ to 9.5‰, which were in the middle of the ranges of $\delta^{15}N$ values for major emission sources (Table S1).

In this study, the contribution of combustion-related sources to the presence of precipitation NH_4^+ in cities reach up to 60% (Fig. 5a). This is consistent with previous results in urban areas that the relative contribution of combustion-related NH_3 to total NH_3 emissions is 55% in Guiyang in Southwest China, 63% in Zhanjiang in Southeast China, 43%–72% in Beijing in North China, 63%–66% in Xi'an in Northwest China, and 55% ± 6% in coastal areas in the USA based on the $\delta^{15}N$ values of NH_3, precipitation NH_4^+, or particulate NH_4^+ (Liu et al., 2017; Wu et al., 2019; Berner and Felix, 2020; Bhattarai et al., 2020; Chen et al., 2020; Wu et al., 2020; Zhang et al., 2020). The relative contribution of combustion-related NH_3 is higher than the contribution of the reporting forest (34% ± 3%) and crop fields (31% ± 12%) (Berner and Felix, 2020; Xu et al., 2021).

The real contribution of combustion-related NH_3 was higher in urban areas than in suburban areas (Fig. 5c), confirming a higher emission strength for combustion-related NH_3 as compared to volatilization NH_3 in urban areas than in suburban areas, which emphasizes the importance of NH_3 emissions from combustion-related sources in urban environments. The wet NH_4^+ deposition from volatilization NH_3 in Yangzhou was higher than the deposition in Nanjing (Fig. 5c), which could be well attributed to the 2 and 1.5 times higher production of meat and grain and fertilization intensity in Yangzhou, respectively (Table S2).

4.4. Major sources of NO_3^- in precipitation

The rainwater $\delta^{15}N_{w\text{-}NO3-}$ values in Nanjing ranged from −17.3‰ to +7.6‰ with an average of −9.0 ± 5.9‰ for SY and −6.5 ± 5.2‰ for XL. These values in Yangzhou ranged from −17.3‰ to 17.8‰ with an average of −1.4 ± 6.3‰ for HHC and −0.2 ± 7.2‰ for YZJ (Fig. 2m–p), which fell within the range of publication $\delta^{15}N_{w\text{-}NO3-}$ values (Song et al., 2021) and $\delta^{15}N$ values for major sources (Table S1).

In the atmosphere, the initial NO_x mixture is partially oxidized to HNO_3 and particulate NO_3^-, and then scavenged as precipitation NO_3^- if precipitation occurred. There were substantial $\delta^{15}N$ differences between ambient NO_x, HNO_3, particulate NO_3^-, precipitation NO_3^-, and initial NO_x mixture due to N isotope fractionation and preferential wet scavenging (Walters and Michalski, 2015; Liu et al., 2020; Song et al., 2021). The $\delta^{15}N$ values of the initial NO_x mixture were estimated on the basis of both the concentrations and $\delta^{15}N$ values of ambient NO_x, HNO_3, and particulate NO_3^-. Then, the $\delta^{15}N$ value difference between precipitation NO_3^- and the initial NO_x mixture was estimated to be 3.9 ± 1.8‰ and can be used to calculate the relative contribution of major sources in East Asia (Song et al., 2021), thus was used in this study.

The results revealed that non-fossil fuel NO_x emissions (biomass burning and microbial N cycle) account for more than 50% of the total NO_x emissions (Fig. 5b). This is consistent with previous results in urban areas that the relative contribution of non-fossil fuel NO_x to total NO_x emissions is 50% in Guiyang and 40% in the Chongqing in Southwest China, 39% in the Shenyang in Northeast China, and 49% ± 11% in East Asia, North America, and Europe (Liu et al., 2017; Li et al., 2019; Cui et al., 2020; Song et al., 2021). However, the relative contribution of non-fossil fuel NO_x at urban/suburban sites below that of non-urban sites in East Asia, North America, and Europe, reported as 66% ± 13%, 69% ± 13%, and 70% ± 12%, respectively (Song et al., 2021). The relative contribution and real contribution of fossil fuel NO_x were higher in Yangzhou than in Nanjing (Fig. 5b & d). Supportively, Yangzhou is dominated by secondary industry, while Nanjing is dominated by tertiary industry (Table S2). The real contribution of non-fossil fuel NO_x was higher in urban areas than in suburban areas, which may be due to NO_x emissions from the microbial N cycle, especially from urban sewage and polluted aquatic ecosystems.

Although the relative contributions of NH_3 and NO_x sources were estimated using the Bayesian model considering the N isotopic effects, there remain some uncertainties regarding the source apportionments, which require further investigation. Firstly, there may be an uncertainty in isotopic effects due to complex secondary atmospheric processes, which would not change the importance of combustion-related NH_3 and non-fossil fuel NO_x, but might specify their relative contributions (Fig. S1). Secondly, the $\delta^{15}N$ values of the sources are still limited and have substantial variability. Thirdly, the SIAR model estimates the probability distribution rather than the precise relative contribution of each source because of the uncertainties in the isotopic effects and $\delta^{15}N$ values of the emission sources.

5. Conclusion

In this study, N species and $\delta^{15}N$ values of rainwater were observed at urban and suburban sites of developed and developing cities to understand the effect of urbanization on N deposition and estimate the sources of precipitation in the city environment. We observed higher deposition rates and considerable spatial differences in the N deposition rate in developing cities than those in developed cities; in urban areas, these parameters were higher than those in suburban areas. The spatial variation of NH_4^+/NO_3^- was similar to that of N deposition, both reflecting the impact of urbanization on N deposition and urban combustion-related NH_3 emissions. $\delta^{15}N_{w\text{-}NH4+}$ was found to increase with the increase in precipitation pH values because of the effects of atmospheric neutralization conditions on the equilibrium reaction between NH_3 and particulate NH_4^+ and wet scavenging of NH_3 and particulate NH_4^+. The quantitative results from SIAR showed that NH_3 from combustion-related sources (coal combustion, vehicle exhaust, and biomass burning) more than volatilization sources (fertilizer application and waste volatilization), and NO_x from non-fossil fuel combustion (biomass burning and microbial N cycle) is comparable to fossil-fuel combustion (coal combustion and vehicle exhaust) in city areas. The results highlighted the emission of combustion-related NH_3 and non-fossil fuel NO_x in city areas, which is useful for understanding the

sources of N deposition and effectively reducing reactive N emissions and air pollution.

CRediT authorship contribution statement

Z.C. and T.H. designed the research. Z.C., X.H., and Y.Y. conducted the research (sampling, laboratory analyses, data analyses). Z.C. and T.H. co-wrote the paper, with contributions from other authors.

Data and materials availability

All data needed to evaluate the conclusions in the paper are present in the paper and/or the Supplementary Information. Additional data related to this paper may be requested from the authors.

Declaration of competing interest

The authors declare no competing financial interests.

Acknowledgements

This work was funded by the National Natural Science Foundation of China [Grant numbers 41571324, 41771340, and 41701329]; the Youth Top Talent funded by Nanjing Normal University, National Program on Key Basic Research Project (973 Program) [grant number 2014CB953800]; the Natural Science Foundation of the Jiangsu Higher Education Institutions of China [grant number 16KJD170001]; the Natural Science Foundation of Hainan Province, China [grant number 317190]; the Key R&D Plan program of Jiangsu Province [grant number BE2020319]; and the CAGS Research Fund [grant numbers YYWF201637, 201724]. We would like to thank Editage (www.editage.cn) for English language editing.

Appendix A. Supplementary data

Supplementary data to this article can be found online at https://doi.org/10.1016/j.scitotenv.2021.150502.

References

Aikawa, M., Hiraki, T., 2009. Washout/rainout contribution in wet deposition estimated by 0.5 mm precipitation sampling/analysis. Atmos. Environ. 43, 4935–4939.
Almaraz, M., Bai, E., Wang, C., Trousdell, J., Conley, S., Faloona, I., Houlton, B.Z., 2018. Agriculture is a major source of NOx pollution in California. Sci. Adv. 4 (6), 1–9.
Anenberg, S.C., Miller, J., Minjares, R., Du, L., Henze, D.K., Lacey, F., 2017. Impacts and mitigation of excess diesel-related NOx emissions in 11 major vehicle markets. Nature 545, 467–471.
Berner, A.H., Felix, J.D., 2020. Investigating ammonia emissions in a coastal urban airshed using stable isotope techniques. Sci. Total Environ. 707, 134952.
Bhattarai, N., Wang, S., Xu, Q., Dong, Z., Chang, X., Jiang, Y., Zheng, H., 2020. Sources of gaseous NH3 in urban Beijing from parallel sampling of NH3 and NH4+, their nitrogen isotope measurement and modeling. Sci. Total Environ. 747, 141361.
Cao, T.T.H., Nakamura, T., Saiki, M., Ta, T.T., Toyama, T., Nishida, K., 2018. Effect of dissolved organic nitrogen contamination on δ15N-NH4 determination in water samples by modification of the diffusion method with gas-phase trapping. Rapid. Commun. Mass. Spectrom. 32 (8), 635–638.
Chang, Y.H., 2014. Non-agricultural ammonia emissions in urban China. Atmos. Chem. Phys. Discuss. 14 (6), 8495–8531.
Chang, Y.H., Deng, C.R., Dore, A.J., Zhuang, G.S., 2015. Human excreta as a stable and important source of atmospheric ammonia in the megacity of Shanghai. PLoS One 10 (12), e0144661.
Chang, Y.H., Liu, X.J., Deng, C.R., Dore, A.J., Zhuang, G.S., 2016b. Source apportionment of atmospheric ammonia before, during, and after the 2014 APEC summit in Beijing using stable nitrogen isotope signatures. Atmos. Chem. Phys. 16 (18), 11635–11647.
Chang, Y.H., Zou, Z., Deng, C.R., Huang, K., Collett, J.L., Lin, J., Zhuang, G.S., 2016a. The importance of vehicle emissions as a source of atmospheric ammonia in the megacity of Shanghai. Atmos. Chem. Phys. 16 (5), 3577–3594.
Chen, Z.L., Huang, T., Huang, X.H., Han, X.X., Yang, H., Cai, Z.C., Yao, L., Han, X., Zhang, M.G., Huang, C.C., 2019. Characteristics, sources and environmental implications of atmospheric wet nitrogen and sulfur deposition in Yangtze River Delta. Atmos. Environ. 219, 116904.
Chen, F., Lao, Q., Li, Z., Bian, P., Zhu, Q., Chen, C., Song, Z., 2020. Monthly variations of the nitrogen isotope of ammonium in wet deposition in a tropical city of South China. Aerosol Air Qual. Res. 20 (5), 1062–1069.
Cui, J., Zhou, F.W., Gao, M., Zhang, L.Y., Zhang, L.M., Du, K., Leng, Q.M., Zhang, Y.Z., He, D.Y., Yang, F.M., Chan, A., 2018. A comparison of various approaches used in source apportionments for precipitation nitrogen in a mountain region of Southwest China. Environ. Pollut. 241, 810–820.
Cui, J., Zhang, Y.Z., Yang, F.M., Chang, Y.J., Du, K., Chan, A., Yao, D.R., 2020. Seasonal fluxes and sources apportionment of dissolved inorganic nitrogen wet deposition at different land-use sites in the Three Gorges reservoir area. Ecotox. Environ. Safe. 193, 110344.
Davis, P., Syme, J., Heikoop, J., Fessenden-Rahn, J., Perkins, G., Newman, B., Chrystal, A.E., Hagerty, S.B., 2015. Quantifying uncertainty in stable isotope mixing models. J. Geophys. Res. Biogeosci. 120, 903–923.
Decina, S.M., Hutyra, L.R., Templer, P.H., 2019. Hotspots of nitrogen deposition in the world's urban areas: a global data synthesis. Front. in Ecol. Environ. 18 (2), 92–100.
Delwiche, C.C., Steyn, P.L., 1970. Nitrogen isotope fractionation in soils and microbial reactions. Environ. Sci. Technol. 4, 929–935.
Du, F., 2012. Inorganic Sulfur and Nitrogen Isotope Variation in Atmospheric Precipitation at Chengdu. China Chengdu University of Technology, Chengdu.
Du, E.Z., de Vries, W., Galloway, J.N., Hu, X.Y., Fang, J.Y., 2014. Changes in wet nitrogen deposition in the United States between 1985 and 2012. Environ. Res. Lett. 9 (9), 095004.
Elliott, E.M., Yu, Z.J., Cole, A.S., Coughlin, J.G., 2019. Isotopic advances in understanding reactive nitrogen deposition and atmospheric processing. Sci. Total Environ. 662, 393–403.
Evans, M., Hastings, N., Peacock, B., 2000. Statistical Distributions. third edn. John Wiley and Sons, New York.
Fowler, D., Coyle, M., Skiba, U., Sutton, M.A., Cape, J.N., Reis, S., Sheppard, L.J., Jenkins, A., Grizzetti, B., Galloway, J.N., Vitousek, P., Leach, A., Bouwman, A.F., Butterbach-Bahl, K., Dentener, F., Stevenson, D., Amann, M., Voss, M., 2013. The global nitrogen cycle in the twenty-first century. Phil. Trans. Roy. Soc. B-Biol. Sci. 368 (1621), 20130164.
Fu, X., Wang, S.X., Zhao, B., Xing, J., Cheng, Z., Liu, H., Hao, J.M., 2013. Emission inventory of primary pollutants and chemical speciation in 2010 for the Yangtze River Delta region, China. Atmos. Environ. 70, 39–50.
Galloway, J.N., Townsend, A.R., Erisman, J.W., Bekunda, M., Cai, Z.C., Freney, J.R., Martinelli, L.A., Seitzinger, S.P., Sutton, M.A., 2008. Transformation of the nitrogen cycle: recent trends, questions, and potential solutions. Science 320 (5878), 889–892.
Gao, Y., 2002. Atmospheric nitrogen deposition to Barnegat Bay. Atmos. Environ. 36, 5783–5794.
Gu, B.J., Ju, X.T., Chang, J., Ge, Y., Vitousek, P.M., 2015. Integrated reactive nitrogen budgets and future trends in China. Proc. Natl. Acad. Sci. U. S. A. 112 (28), 8792–8797.
Hanschmann, G., 1981. Berechnung von isotopieeffekten auf quantenchemischer grundlage am beispiel sticksoffhaltiger molekule. ZFI-Mitt. 41, 19–39.
Hayasaka, H., Fukuzaki, N., Kondo, S., Ishizuka, T., Totsuka, T., 2004. Nitrogen isotopic ratios of gaseous ammonia and ammonium aerosols in the atmosphere. J. Jpn. Soc. Atmos. Environ. 39, 272–279.
Heaton, T.H.E., Spiro, B., Robertson, S.M.C., 1997. Potential canopy influences on the isotopic composition of nitrogen and sulphur in atmospheric deposition. Oecologia 109 (4), 600–607.
Högberg, P., 1997. 15N natural abundance in soil-plant systems. New Phytol. 137, 179–203.
Holland, E.A., Braswell, B.H., Sulzman, J., Lamarque, J.F., 2005. Nitrogen deposition onto the United States and Western Europe: synthesis of observations and models. Ecol. Appl. 15 (1), 38–57.
Huang, C., Chen, C.H., Li, L., Cheng, Z., Wang, H.L., Huang, H.Y., Streets, D.G., Wang, Y.J., 2011. The study of emission inventory on anthropogenic air pollutants and VOC species in the Yangtze River Delta region, China. Atmos. Chem. Phys. Discuss. 11 (1), 951–983.
Huang, S.N., Elliott, E.M., Felix, J.D., Pan, Y.P., Liu, D.W., Li, S.L., Li, Z.J., Zhu, F.F., Zhang, N., Fu, P.Q., Fang, Y.T., 2019. Seasonal pattern of ammonium 15N natural abundance in precipitation at a rural forested site and implications for NH3 source partitioning. Environ. Pollut. 247, 541–549.
Jaeglé, L., Steinberger, L., Martin, R.V., Chance, K., 2005. Global partitioning of NOx sources using satellite observations: relative roles of fossil fuel combustion, biomass burning and soil emissions. Faraday Discuss. 130, 407–423.
Jain, A.K., Tao, Z.N., Yang, X.J., Gillespie, C., 2006. Estimates of global biomass burning emissions for reactive greenhouse gases (CO, NMHCs, and NOx) and CO2. J. Geophys. Res. Atmos. 111, D06304.
Kawashima, H., 2019. Seasonal trends of the stable nitrogen isotope ratio in particulate nitrogen compounds and their gaseous precursors in Akita, Japan. Tellus B 71, 1–13.
Kawashima, H., Ono, S., 2019. Nitrogen isotope fractionation from ammonia gas to ammonium in particulate ammonium chloride. Environ. Sci. Technol. 53 (18), 10629–10635.
Lee, K.S., Lee, D.S., Lim, S.S., Kwak, J.H., Jeon, B.J., Lee, S.I., Lee, S.M., Choi, W.J., 2012. Nitrogen isotope ratios of dissolved organic nitrogen in wet precipitation in a metropolis surrounded by agricultural areas in southern Korea. Agric. Ecosyst. Environ. 159, 161–169.
Leng, Q.M., Cui, J., Zhou, F.W., Du, K., Zhang, L.Y., Fu, C., Liu, Y., Wang, H.B., Shi, G.M., Gao, M., Yang, F.M., He, D.Y., 2018. Wet-only deposition of atmospheric inorganic nitrogen and associated isotopic characteristics in a typical mountain area, southwestern China. Sci. Total Environ. 616–617, 55–63.
Li, J., Fang, Y.T., Yoh, M., Wang, X.M., Wu, Z.Y., Kuang, Y.W., Wen, D.Z., 2012b. Organic nitrogen deposition in precipitation in metropolitan Guangzhou city of southern China. Atmos. Res. 113, 57–67.
Li, L., Lollar, B.S., Li, H., Wortmann, U.G., Lacrampe-Couloume, G., 2012a. Ammonium stability and nitrogen isotope fractionations for NH4+–NH3(aq)–NH3(gas) systems at 20–70°C and pH of 2–13: applications to habitability and nitrogen cycling in low-temperature hydrothermal systems. Geochim. Cosmochim. Acta 84, 280–296.

Li, Y., Schichetl, B.A., Walker, J.T., Schwede, D.B., Chen, X., Lehmann, C.M.B., Puchalski, M.A., Gay, D.A., Collett Jr., J.L., 2016. Increasing importance of deposition of reduced nitrogen in the United States. Proc. Natl. Acad. Sci. U. S. A. 113, 5874–5879.
Li, Z.J., Walters, W.W., Hastings, M.G., Zhang, Y.L., Song, L.L., Liu, D.W., Zhang, W.Q., Pan, Y.P., Fu, P.Q., Fang, Y.T., 2019. Nitrate isotopic composition in precipitation at a Chinese megacity: seasonal variations, atmospheric processes, and implications for sources. Earth Space Sci. 6 (11), 2200–2213.
Liu, X.J., Zhang, Y., Han, W.X., Tang, A.H., Shen, J.L., Cui, Z.L., Vitousek, P., Erisman, J.W., Goulding, K., Christie, P., Fangmeier, A., Zhang, F.S., 2013. Enhanced nitrogen deposition over China. Nature 494 (7438), 459–462.
Liu, D.W., Fang, Y.T., Tu, Y., Pan, Y.P., 2014. Chemical method for nitrogen isotopic analysis of ammonium at natural abundance. Anal. Chem. 86 (8), 3787–3792.
Liu, X.Y., Xiao, H.W., Xiao, H.Y., Song, W., Sun, X.C., Zheng, X.D., Liu, C.Q., Koba, K., 2017. Stable isotope analyses of precipitation nitrogen sources in Guiyang, southwestern China. Environ. Pollut. 230, 486–494.
Liu, X.Y., Yin, Y.M., Song, W., 2020. Nitrogen isotope differences between major atmospheric NOy species: implications for transformation and deposition processes. Environ. Sci. Technol. Lett. 7 (4), 227–233.
Lu, C.Q., Tian, H.Q., 2014. Half-century nitrogen deposition increase across China: a gridded time-series data set for regional environmental assessments. Atmos. Environ. 97, 68–74.
Luo, L.C., Qin, B.Q., Song, Y.Z., Yang, L.Y., 2007. Seasonal and regional variations in precipitation chemistry in the Lake Taihu Basin, China. Atmos. Environ. 41 (12), 2674–2679.
Martin, R.V., 2003. Global inventory of nitrogen oxide emissions constrained by space-based observations of NO2 columns. J. Geophys. Res. Atmos. 108, 1–12.
Meng, W.J., Zhong, Q.R., Yun, X., Zhu, X., Huang, T.B., Shen, H.Z., Chen, Y.L., Chen, H., Zhou, F., Liu, J.F., Wang, X.M., Zeng, E.Y., Tao, S., 2017. Improvement of a global high-resolution ammonia emission inventory for combustion and industrial sources with new data from the residential and transportation sectors. Environ. Sci. Technol. 51 (5), 2821–2829.
Mizak, C.A., Campbell, S.W., Luther, M.E., Carnahan, R.P., Murphy, R.J., Poor, N.D., 2005. Below-cloud ammonia scavenging in convective thunderstorms at a coastal research site in Tampa, FL, USA. Atmos. Environ. 39, 1575–1584.
Moore, H., 1977. Isotopic composition of ammonia, nitrogen-dioxide and nitrate in atmosphere. Atmos. Environ. 11 (12), 1239–1243.
Moore, J.W., Semmens, B.X., 2008. Incorporating uncertainty and prior information into stable isotope mixing models. Ecol. Lett. 11, 470–480.
Oberholzer, B., Volken, M., Collett, J.L., Staehenlin, J., Waldvogel, A., 1993. Pollutant concentrations and below-cloud scavenging of selected N (-III) species along a mountain slope. Water Air Soil Pollut. 68 (1), 59–73.
Ohara, T., Akimoto, H., Kurokawa, J., Horii, N., Yamaji, K., Yan, X., Hayasaka, T., 2007. An Asian emission inventory of anthropogenic emission sources for the period 1980–2020. Atmos. Chem. Phys. 7, 4419–4444.
Pan, Y.P., Tian, S.L., Liu, D.W., Fang, Y.T., Zhu, X.Y., Gao, M., Gao, J., Michalski, G., Wang, Y.S., 2018b. Isotopic evidence for enhanced fossil fuel sources of aerosol ammonium in the urban atmosphere. Environ. Pollut. 238, 942–947.
Pan, Y.P., Tian, S.L., Zhao, Y.H., Zhang, L., Zhu, X.Y., Gao, J., Huang, W., Zhou, Y.B., Song, Y., Zhang, Q., Wang, Y.S., 2018a. Identifying ammonia hotspots in China using a national observation network. Environ. Sci. Technol. 52 (7), 3926–3934.
Pan, Y.P., Gu, M.N., Song, L.L., Tian, S.L., Wu, D.M., Walters, W.W., Yu, X.N., Lü, X.M., Ni, X., Wang, Y.J., Cao, J., Liu, X.J., Fang, Y.T., Wang, Y.S., 2020. Systematic low bias of passive samplers in characterizing nitrogen isotopic composition of atmospheric ammonia. Atmos. Res. 243, 105018.
Parnell, A., Jackson, A., 2008. SIAR: Stable isotope analysis in R. http://cran.r-project.org/web/packages/siar/index.html. (Accessed 12 October 2008).
Qiao, X., Xiao, W.Y., Jaffe, D., Kota, S.H., Ying, Q., Tang, Y., 2015. Atmospheric wet deposition of sulfur and nitrogen in jiuzhaigou National Nature Reserve, Sichuan Province, China. Sci. Total Environ. 511, 28–36.
Seinfeld, J.H., Pandis, S.N., 2006. Atmospheric Chemistry and Physics: From Air Pollution to Climate Change. 2nd Ed. John Wiley & Sons, New York.
Shao, W., Zhang, Y., Song, L., Jia, J.Y., Liu, X.J., Cai, X.B., 2009. Atmospheric organic nitrogen deposition in Linzhi area, Tibet. Acta Ecol. Sinica 29 (10), 5586–5591.
Shen, B.N., Zhang, L.Y., Yang, F.M., 2017. Characteristics of pH value and conductivity of precipitation in the hinterland of the Three Gorges Reservoir, China. Yunnan Geogr. Environ. Res. 29 (4), 24–32.
Shimshock, J.P., Pena, R.G.D., 1988. Below-cloud scavenging of tropospheric ammonia. Tellus B. 41B (3), 296–304.
Sigman, D.M., Altabet, M.A., Michener, R., McCorkle, D.C., Fry, B., Holmes, R.M., 1997. Natural abundance-level measurement of the nitrogen isotopic composition of oceanic nitrate- an adaptation of the ammonia diffusion method. Mar. Chem. 57, 227–242.
Song, W., Liu, X.Y., Hu, C.C., Chen, G.Y., Liu, X.J., Walters, W.W., Michalski, G., Liu, C.Q., 2021. Important contributions of non-fossil fuel nitrogen oxides emissions. Nat. Commun. 12 (1), 243.
Ti, C.P., Gao, B., Luo, Y.X., Wang, X., Wang, S.W., Yan, X.Y., 2018. Isotopic characterization of NHx-N in deposition and major emission sources. Biogeochemistry 138 (1), 85–102.
Urey, H.C., 1947. The thermodynamic properties of isotopic substances. J. Chem. Soc. 562–581.
Walters, W.W., Michalski, G., 2015. Theoretical calculation of nitrogen isotope equilibrium exchange fractionation factors for various NOy molecules. Geochim. Cosmochim. Acta 164, 284–297.
Walters, W.W., Chai, J., Hastings, M.G., 2019. Theoretical phase resolved ammonia–ammonium nitrogen equilibrium isotope exchange fractionations: applications for tracking atmospheric ammonia gas-to-particle conversion. ACS Earth Space Chem. 3 (1), 79–89.
Walters, W.W., Song, L.L., Chai, J.J., Fang, Y.T., Colombi, N., Hastings, M.G., 2020. Characterizing the spatiotemporal nitrogen stable isotopic composition of ammonia in vehicle plumes. Atmos. Chem. Phys. 20, 11551–11567.
Wang, Y.L., Liu, X.Y., Song, W., Yang, W., Han, B., Dou, X.Y., Zhao, X.D., Song, Z.L., Liu, C.Q., Bai, Z.P., 2017. Source appointment of nitrogen in PM2.5 based on bulk δ15N signatures and a bayesian isotope mixing model. Tellus B. 69 (1), 1299672.
Wu, L., Ren, H., Wang, P., Chen, J., Fang, Y., Hu, W., Ren, L., Deng, J., Song, Y., Li, J., Sun, Y., Wang, Z., Liu, C.Q., Ying, Q., Fu, P., 2019. Aerosol ammonium in the urban boundary layer in Beijing: insights from nitrogen isotope ratios and simulations in summer 2015. Environ. Sci. Tech. Lett. 6 (7), 389–395.
Wu, C., Wang, G., Li, J., Li, J., Cao, C., Ge, S., Xie, Y., Chen, J., Liu, S., Du, W., Zhao, Z., Cao, F., 2020. Non-agricultural sources dominate the atmospheric NH3 in Xi'an, a megacity in the semi-arid region of China. Sci. Total Environ. 722, 137756.
Xiao, H.W., Xiao, H.Y., Long, A.M., Wang, Y.L., 2012. Who controls the monthly variations of NH4+ nitrogen isotope composition in precipitation? Atmos. Environ. 54, 201–206.
Xiao, H.W., Xiao, H.Y., Long, A.M., Wang, Y.L., Liu, C.Q., 2013. Chemical composition and source apportionment of rainwater at Guiyang, SW China. J. Atmos. Chem. 70 (3), 269–281.
Xiao, H.W., Xiao, H.Y., Long, A.M., Liu, C.Q., 2015. δ15N–NH4+ variations of rainwater: application of the Rayleigh model. Atmos. Res. 157, 49–55.
Xu, Z.F., Han, G.L., 2009. Chemical and strontium isotope characterization of rainwater in Beijing China. Atmos. Environ. 43 (12), 1954–1961.
Xu, S.Y., Huang, H., Song, W., Liu, X.Y., 2021. Lichen nitrogen concentrations and isotopes for indicating nitrogen deposition levels and source changes. Sci. Total Environ. 787, 147616.
Yu, G.R., Jia, Y.L., He, N.P., Zhu, J.X., Chen, Z., Wang, Q.F., Piao, S.L., Liu, X.J., He, H.L., Guo, X.B., Wen, Z., Li, P., Ding, G.A., Goulding, K., 2019. Stabilization of atmospheric nitrogen deposition in China over the past decade. Nat. Geosci. 12 (6), 424–429.
Zhang, Y., Liu, X.J., Zhang, F.S., Ju, X.T., Zou, G.Y., Hu, K.L., 2006. Spatial and temporal variation of atmospheric nitrogen deposition in the North China Plain. Acta Ecol. Sin. 26 (6), 1633–1638.
Zhang, P.Y., Wen, T., Zhang, J.B., Cai, Z.C., 2017. On improving the diffusion method for determination of δ15N-NH4+ and δ15N-NO3- in soil extracts. Acta Pedol. Sin. 54 (4), 948–957.
Zhang, Y.Y., Benedict, K.B., Tang, A.H., Sun, Y., Fang, Y.L., Liu, X.J., 2020. Persistent nonagricultural and periodic agricultural emissions dominate sources of ammonia in urban Beijing: evidence from 15N stable isotope in vertical profiles. Environ. Sci. Technol. 54, 102–109.
Zheng, X.D., Liu, X.Y., Song, W., Sun, X.C., Liu, C.Q., 2018. Nitrogen isotope variations of ammonium across rain events: implications for different scavenging between ammonia and particulate ammonium. Environ. Pollut. 239, 392–398.